Analyzing buckling mode interactions in elastic structures using an asymptotic approach: theory and experiments

Pergamon

Computers & Structures Vol. 64, No. 1–4, pp. 473–480, 1997

Printed in Great Britain
0045-7949/97 $17.00 + 0.00

PII: S0045-7949(96)00139-3

ANALYZING BUCKLING MODE INTERACTIONS IN ELASTIC STRUCTURES USING AN ASYMPTOTIC APPROACH; THEORY AND EXPERIMENTS

C. M. Menken, G. M. A. Schreppers, W. J. Groot and **R. Petterson**
Eindhoven University of Technology, P.O. Box 513, 5600 MB Eindhoven, The Netherlands

Abstract—This paper describes the theoretical basis of a computer program for analyzing the buckling and initial post-buckling behavior of prismatic plate structures. Post-buckling behavior is described in terms of the amplitudes of a limited number of skilfully chosen buckling modes. Experiments were carried out to validate the program. The rarely investigated problem of interaction between overall lateral-torsional buckling and local buckling was chosen as a test case. © 1997 Civil-Comp Ltd and Elsevier Science Ltd.

1. INTRODUCTION

The post-buckling behavior of thin-walled structures is very complex and the simple Euler type of buckling is an exception. This complexity is caused by a multitude of nearly coincident critical loads occurring in the numerical models for a perfect structure, the perfect structure being the basis for the calculation of a real, imperfect structure. The modes may couple (interact) in a non-linear way, either directly at the first critical point, or later at a secondary bifurcation (sec. bif.) of the already bifurcated post-buckling path. These phenomena were comprehensively described by Thompson and Hunt [1] for simple discrete models, and by Koiter [2] for continua. These authors showed the destabilizing influence of coupling of modes. As a simple example, Augusti [3] presented a two-mode model having two stable uncoupled post-buckling equilibrium paths, but having unstable coupled equilibrium paths. The real structure will follow the latter path approximately. That mode interaction is the reason why the numerical modeling of real thin-walled structures, having many buckling modes, is very difficult [4] and requires a good knowledge of buckling behavior. Moreover, most computer codes are based on the finite element method, which involves a large number of unknowns, and it traces an equilibrium path in a stepwise manner involving all these unknowns. As a consequence, such numerical modeling requires considerable computing time.

In order to reduce computing time, a computer program was developed for prismatic plate structures, such as longitudinally stiffened panels, folded plate structures and built-up girders [5]. That program combines Byskov and Hutchinson's [6] modification of Koiter's [7] asymptotic post-buckling theory with a spline finite element formulation. According to that theory, the initial post-buckling displacements can be described primarily by a linear combination of buckling modes, augmented with some second order fields. Preliminary numerical and experimental results [8] suggested that a limited number of modes would suffice, which implies that the initial post-buckling behavior can be described by a small set of non-linear equilibrium equations, the number of equations being equal to the number of modes chosen. Subsequently the stepwise method can be used with fewer equations rather than with all the unknowns, as is usually the case with the full finite element approach. Moreover, using (selected) modes gives a better insight into the actual buckling problem before dealing with all the displacements. In order to validate the reasoning behind such a program, we performed some buckling experiments that displayed mode interactions, and compared the results with numerical simulations of the experiments. We chose the problem of interaction between overall lateral-torsional buckling (OB) and local flange buckling (LB) of a simple supported thin-walled T-beam subjected to a transverse force at midspan.

2. AN OUTLINE OF THE ASYMPTOTIC APPROACH

A finite element program was developed for analyzing the initial post-buckling behavior (after the linear pre-buckling behavior of the perfect structure) of elastic prismatic plate structures under conservative loading. The post-buckling formulation of Byskov and Hutchinson [6] was used, because it is not restricted to nearly coincident critical loads like Koiter's original theory. From experiments it was found that even modes pertaining to well-separated critical loads may lead to interaction [8]. Details of the asymptotic approach are given in Refs [2, 6, 9]. The system is described by a total Lagrangian

expression for the increase of the potential energy when leaving the unbuckled path and, since Lagrange strains include quadratic displacement terms, the potential energy expression will contain second, third and fourth order displacement terms.

The first step involves determining a preselected number of bifurcation loads and their relevant modes. Since bifurcation points are characterized by the vanishing of the quadratic part of the potential energy, this results in the solution of the linear, generalized eigenvalue problem:

$$(\mathbf{K} + \lambda\mathbf{G})\mathbf{u} = \mathbf{0} \tag{1}$$

where $\mathbf{K}$ is the stiffness matrix, λ the load factor, $\mathbf{G}$ the geometric stiffness matrix and $\mathbf{u}$ a buckling mode. The modes are normalized according to:

$$\mathbf{u}_i^{\mathrm{T}}\,\mathbf{K}\mathbf{u}_j = \delta_{ij}. \tag{2}$$

Such a step is found in most buckling analyses. In the present case, however, the buckling modes that were expected to be relevant for the buckling problem at hand have to be selected.

For the post-buckling analysis the full (quartic) potential energy expression is needed and according to the asymptotic theory, the initial post-buckling field $\Delta\mathbf{u}$ can be written as:

$$\Delta\mathbf{u} = a_i\mathbf{u}_i + a_i a_j\mathbf{u}(\lambda)_{ij}, \tag{3}$$

where the second-order fields $\mathbf{u}_{ij}$ and the amplitudes a_i still have to be determined. The contribution of the second-order fields is assumed to be small in comparison with the first-order contribution of the modes.

The second step involves determination of the second-order fields $\mathbf{u}_{ij}$ at fixed amplitudes a_i. Although in Byskov's formulation the $\mathbf{u}_{ij}$ are a function of the load parameter λ, they are determined at a fixed perturbation load λ_p in the vicinity of the lower critical load λ_1. Orthogonality conditions have to be imposed:

$$\mathbf{u}_k^{\mathrm{T}}\,\mathbf{K}\,\mathbf{u}_{ij} = 0. \tag{4}$$

Such constraints can be taken into account conveniently by means of Lagrange multipliers. Since the resulting Lagrangian function must be stationary, the following equations will result:

$$\begin{bmatrix} \mathbf{K} + \lambda_p\mathbf{G} & \mathbf{M} \\ \mathbf{M}^{\mathrm{T}} & 0 \end{bmatrix}\begin{bmatrix} \mathbf{u}_{ij} \\ \mathbf{p}_{ij} \end{bmatrix} = \begin{bmatrix} \mathbf{f}_{ij} \\ 0 \end{bmatrix}. \tag{5}$$

The vector $\mathbf{p}_{ij}$ contains the multipliers relevant to the $\mathbf{u}_{ij}$, while the "load vectors" $\mathbf{f}_{ij}$ result from the potential energy expression which now includes the cubic and quartic terms. The appearance of the stability matrix $(\mathbf{K} + \lambda_p\mathbf{G})$ in those equations indicates that solving eqn (5) will require specific care if λ_p is close to one of the critical loads λ_i. Kouhia and Menken [10] described an iterative procedure for solving eqn (5), which utilizes the fact that the multipliers will be known in advance. After solving the second order fields, the potential energy, V, is still only a function of the amplitudes a_i and the load parameters λ, and is of the form:

$$V[a_i;\ \lambda] = \frac{1}{2}\sum_{I=1}^{m}\left(1 - \frac{\lambda}{\lambda_I}\right)a_I a_I + A_{ijk}a_i a_j a_k + A_{ijkl}a_i a_j a_k a_l, \tag{6}$$

where m equals the number of modes.

The third step now involves solving the equilibrium (amplitude) equations generated from eqn (6) by means of a continuation method. In the case of a compound bifurcation (an exception in numerical analysis) or of a secondary bifurcation, the equilibrium path with the steepest descent or smallest ascent has to be followed.

If it is admissible to insert a small number of modes into eqn (3), the finite element model comprising many degrees of freedom would be reduced for the post-buckling analysis to a very simple model, as described by eqn (6). This simple model would make the problem more tractable for interpretation; the mixed coefficients A_{ijk} and/or A_{ijkl}, for instance, indicating whether there is coupling between buckling modes or not. Moreover, the program allows concentration on the most important coupling by neglecting small coupling terms; the latter being defined by the user.

3. NUMERICAL MODELING

The classical Kirchhoff–Love plate model is used. All the displacement quantities are interpolated by the basic B3-splines in the longitudinal direction. In the transverse direction, cubic Hermitian polynomials are used for approximating the out-of-plane displacements, while in-plane displacements are approximated linearly. The splines guarantee C^1 continuity when modeling folded plate structures. Implementation of the asymptotic approach into a spline finite-strip program has been described by van Erp [9], while Kouhia and Menken [11] implemented it with spline elements.

In this paper, the method is applied to thin-flanged T-beams. The T-beams were modeled with four strips for the web and 10 strips for the flange.

The next part of this section will illustrate how knowledge of the buckling problem can be used to produce a simple numerical model.

Firstly, the classical eigenvalue problem (1) has to be solved for a previously chosen number of critical loads and pertinent modes. That is common to all linearized buckling analyses. From the modes

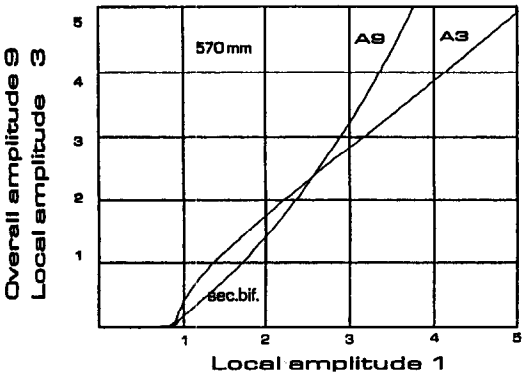

Fig. 1. Relationships between dimensionless post-buckling amplitudes if the smallest critical load initiates local buckling.

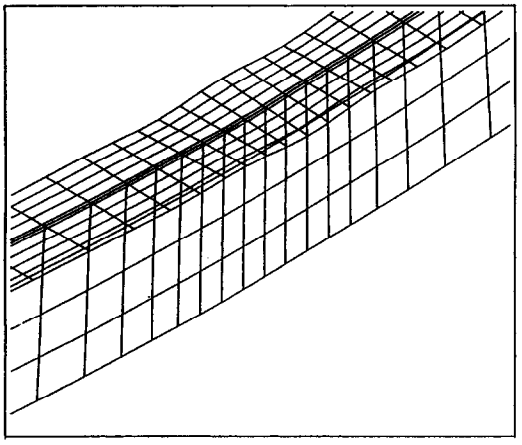

Fig. 3. The shorter beam (570 mm) shows local buckling between the first and second bifurcation point.

obtained, the most appropriate ones should be selected for further analysis. It is obvious that the one pertaining to the lowest buckling load should be the first candidate. It will appear that for the case examined at least two additional modes will be needed for accurately modeling the interactive buckling behavior. If the smallest critical load was a local one, we should look for the first overall one. Conversely, if the smallest was an overall one we should look for a local one.

The following observation from the experiments is important: it appeared that *interaction occurred in all the tested beams, leaving one flange half (the stretched one) free of local buckles!*

Thus, if the smallest local buckling mode is asymmetric with respect to the web, the nearest local mode with almost the same shape in the axial direction, but symmetric with respect to the web, should be chosen and vice versa. Thus, at least three modes are important in the example; however, using only two modes, the second order fields could account for the neglected mode to some extent. Kouhia *et al.* [12] demonstrated that a two mode approach may have a rather limited range of application. After satisfying the choice of modes, the coefficients A_{ijk} and A_{ijkl} that can be ignored shall be selected, in order to simplify the discrete potential energy expression (6).

The last step involves solving the strongly non-linear equilibrium equations obtained from eqn (6), thus giving the amplitudes a_i as functions of the load.

Figures 1 and 2 show the relationships between the dimensionless amplitudes of the numerical models. In Fig. 1, the smallest buckling load is a local one, whereas in Fig. 2 the smallest is an overall one. In both cases, the path related to the smallest critical load is followed initially. At the secondary bifurcation point, the other modes are initiated and, at or somewhere beyond that point (depending on the case), the amplitudes of the local modes become nearly equal. Since the normalized displacements of the local modes [see eqn (2)] are nearly equal, they cancel out each other on one side of the flange, as observed in the experiments. Figures 3–6 show the displacement fields for two different situations, before and after the secondary bifurcation.

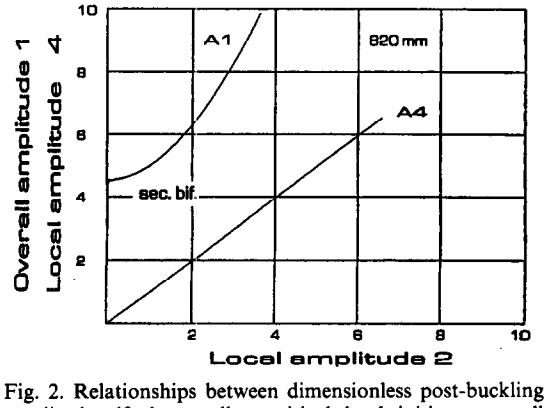

Fig. 2. Relationships between dimensionless post-buckling amplitudes if the smallest critical load initiates overall buckling.

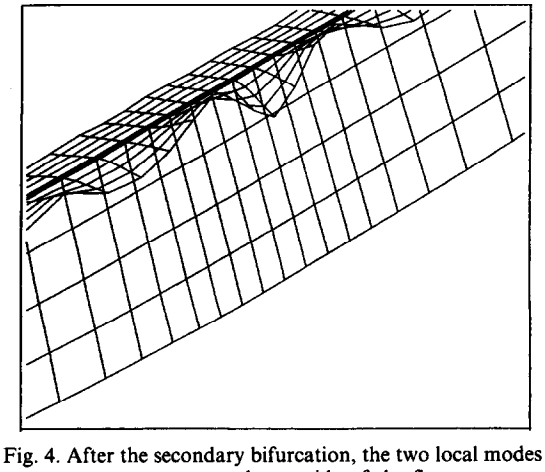

Fig. 4. After the secondary bifurcation, the two local modes cooperate to stretch one side of the flange.

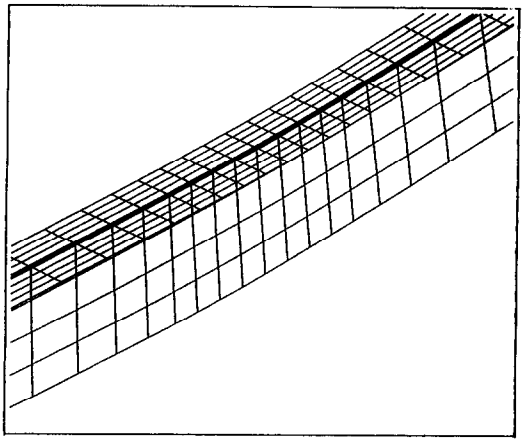

Fig. 5. The longer beam (820 mm) shows overall buckling between the first and second bifurcation point.

4. EXPERIMENTS

Since computing time depends on the number of modes used, an important question is: which are the most relevant modes for an economic, yet proper description of post-buckling behavior? Experiments were carried out in order to get a better insight into this problem as well as to validate the program. Most published experiments relate to pure compression involving periodic (sinusoidal) local buckling [13]. Since the program to be validated allowed arbitrary loading and arbitrary shapes of the buckles, we decided to choose the rarely investigated problem of interaction between overall lateral-torsional buckling and local flange buckling of a simply supported slender T-beam subjected to a concentrated transverse load at midspan. Some researchers have mentioned the scarcity of such experiments [14–16]. The direction of the load induced compression in the flange. This should result in a strongly a-periodic LB in the region of the maximum bending moment.

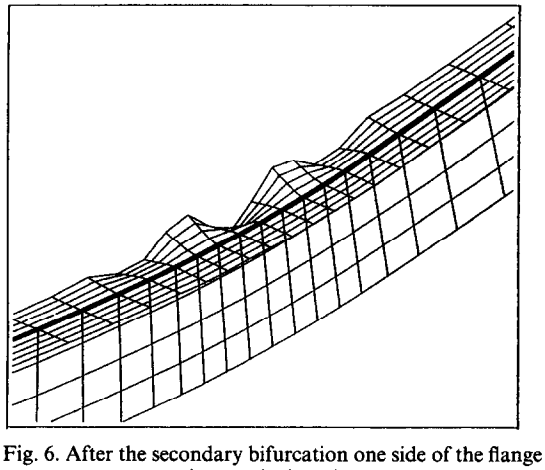

Fig. 6. After the secondary bifurcation one side of the flange is stretched again.

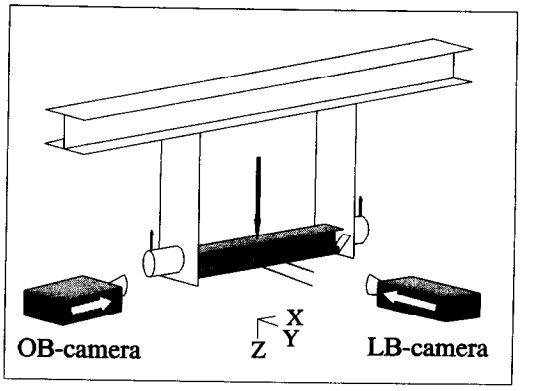

Fig. 7. The test rig.

4.1. *Test specimen*

The aluminium T-beam ($E = 72000\ \mathrm{N\,mm^{-2}}$, $\nu = 0.3$) tested had a thin flange (30×0.5 mm) glued to a relatively thick web (50×2 mm). Although such a combination is rarely seen in engineering practice, it fulfilled our purpose because LB would be predominant in the flange, whereas the web displacements would be representative of OB. Other reasons for choosing a T-beam were:

(1) If only the single flange is in compression, LB of this flange would cause a maximum reduction of the lateral stiffness, resulting in a maximum reduction of the resistance against lateral-torsional buckling. A second flange in tension, as with a H-beam, would diminish that reduction.

(2) As a T-beam does not display primary warping, any uncertainties related to the amount of warping restraint at the supports did not have to be considered.

Altogether six tests were performed in which the length of the beam was the only variable. All dimensions were chosen so that in shorter beams the lowest critical load would initiate local flange buckling, while for the longer beams the lowest critical load would initiate overall lateral-torsional buckling. The beam lengths are given in the figures.

4.2. *Test rig*

Figures 7 and 8 show the test rig. To be able to trace descending equilibrium paths in the post-buckling region, the displacement had to be controlled. Since the load related to the prescribed deflection at midspan and on top of the flange (Fig. 8) had to retain its original direction during the lateral deflection of the beam, the device enforcing this deflection was mounted on a special air bearing, so that it could follow the lateral deflection with negligible friction.

The flexibility of the test rig and its supports made it necessary, in view of the accuracy requirements, to measure the displacements relative to a reference

frame attached to the supported ends of the test specimen.

Displacements were measured contactless with two video cameras tracking the position of about 80 retro-reflective markers, attached to both the test specimen and the reference frame. The markers were illuminated by spotlights mounted around the camera lenses.

Two cameras were used. The first camera ("OB-camera") looked along the axial direction and recorded lateral and vertical displacements of the markers at midspan and in the plane perpendicular to the axis. Those measurements produced the lateral and vertical deflections. The second camera ("LB-camera") looked along the lateral direction and recorded displacements in the x–z plane of the markers attached to the edge of the flange and on the web. That information provided properties of the local buckle. This system permitted displacement measurement accuracy of 0.02 mm approximately.

4.3. *Data acquisition*

Firstly, the observed displacements had to be corrected for known distortions by the cameras themselves and for displacements to and from the cameras (perspective distortion). Using these corrected displacements the following displacements were determined:

(1) The lateral and vertical displacements at the center of gravity of the cross-section at midspan (and not of the point of load application). The lateral displacement was chosen as the OB amplitude and the vertical displacement was used for the load–deflection graph;

(2) The shape of the local buckle (see Fig. 9) was found by comparing the displacements at the edge of the flange with the displacements that would have been observed if the whole flange had remained perpendicular to the web;

(3) The amplitude of the local buckle was determined also from the latter.

The experiments have been described more extensively in another paper [17].

5. A COMPARISON OF THE NUMERICAL AND EXPERIMENTAL RESULTS

The experimental results were compared with the numerical simulations with the aim of validating the program and the idea that the post-buckling behavior can be described with only a few buckling modes. The phenomenon of mode interaction can be understood from the work of Thompson and Hunt [1], the physical events being a reduction in the stiffness together with a stress redistribution and increase in parts of the structure.

There were two major differences between the results of experiments and numerical simulations:

(1) In the experiments, a prescribed displacement first increased and then decreased. That was necessary because a part of the characteristic post-buckling loop, as shown in the load–deflection diagrams of Fig. 10 could only be measured when the displacement decreased. In the numerical simulations, however, the steps for solving the equilibrium equations were all positive.

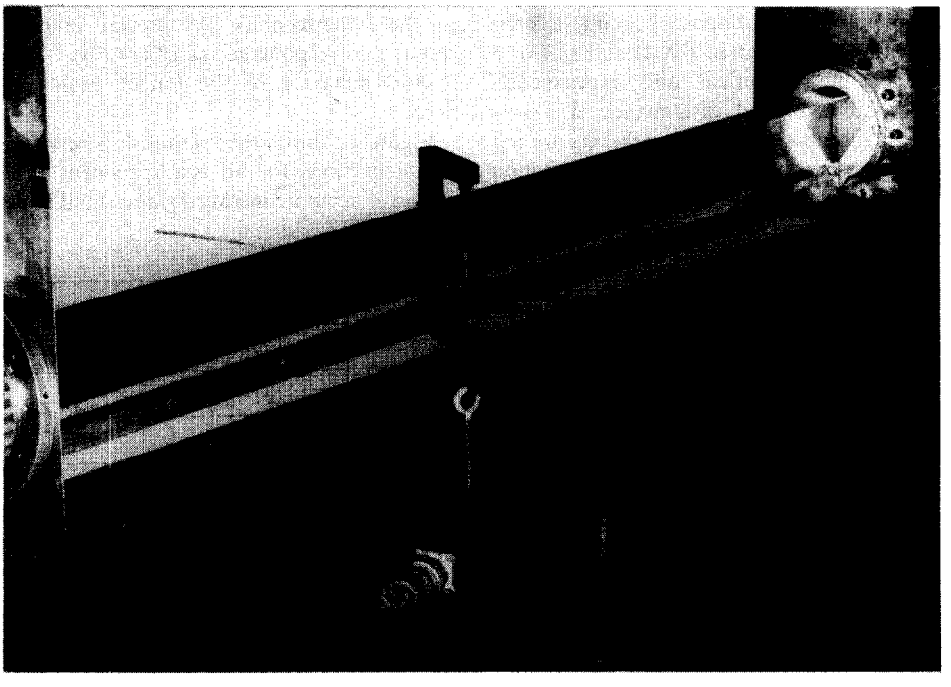

Fig. 8. Photograph of the test rig.

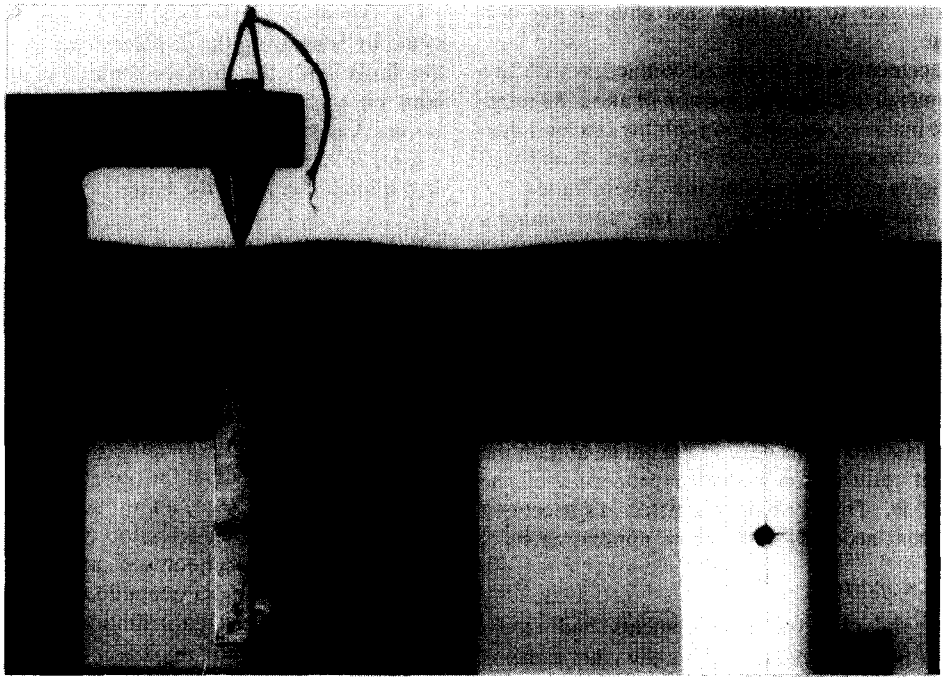

Fig. 9. The local buckle.

(2) In the experiments, both the test specimens and load applications were inevitably imperfect, whereas the numerical simulations used perfect models. The reason for this difference was because geometric imperfections could not be measured without the measuring device imposing displacements in the laterally flexible test specimens. Moreover, the program only accepted imperfections having the shape of a relevant buckling mode. Thus, even if the geometric imperfections were known, it would have been impossible to decompose them into a series of modes for this type of interactive buckling. For a comparison of the numerical and experimental results, the aforementioned discrepancy was surmountable, because these structural members are not very imperfection sensitive although the imperfection could blur details of the initial post-buckling behavior.

Figure 11 shows an example of the experimental relation between OB amplitude and the load. It illustrates that there was always a difference between the path of increasing and decreasing displacements.

Figure 12 shows the relationship between the OB amplitude and the load for both experiments and simulations; the latter showed that secondary bifurcations were involved although they could not be perceived in the experimental results due to the imperfections. At greater amplitudes, the results corresponded satisfactorily. The almost neutral behavior of the longer beams should be noted.

Figure 10 shows the relationship between the load and deflections for all test specimens. The combination of accurate measuring and small imperfections

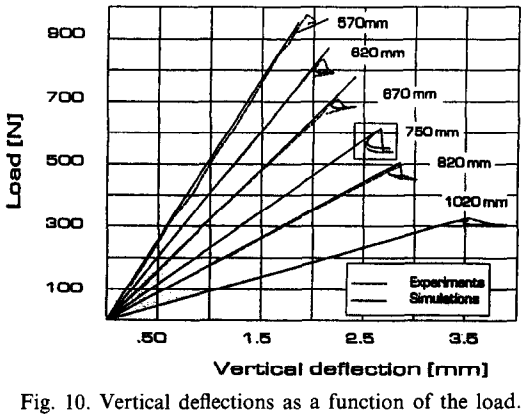

Fig. 10. Vertical deflections as a function of the load.

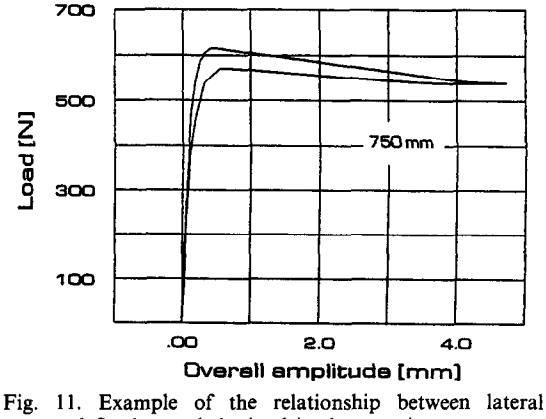

Fig. 11. Example of the relationship between lateral deflection and the load in the experiments.

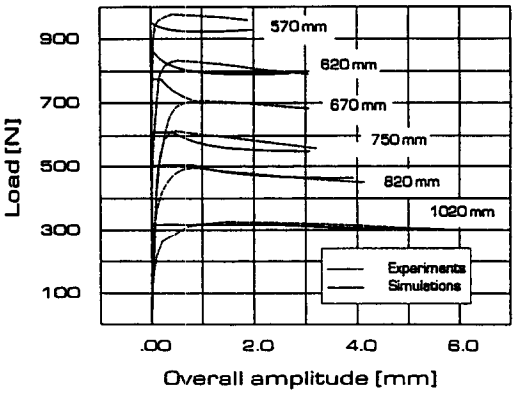

Fig. 12. Lateral deflections (OB amplitudes) as a function of the load.

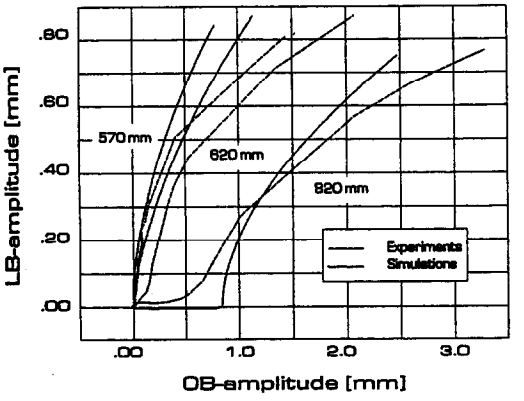

Fig. 14. Relationship between LB and OB amplitudes.

produced parts of the characteristic post-buckling loops, which are particularly evident for the 750 and 820 mm beams. Figure 13 shows a detail of Fig. 10. The solid line represents a numerical simulation with positive steps for solving the equilibrium equations, whilst the broken line represents the experimental results. With a prescribed displacement it is impossible to follow the theoretical curve beyond the secondary bifurcation, the theoretical curve showing a decreasing displacement. Consequently, the load drops with an almost constant deflection. After increasing the deflection still further, it was decreased deliberately in order to obtain part of the loop, albeit with a decreasing deflection. Notwithstanding, the vertical difference between the simulation and the experimental values is less then 2%. It can be concluded from Fig. 11 that positive steps in the numerical simulation and a prescribed reversed displacement in the experiment could never give the same results.

Most of the literature [18] presents relationships that are comparable with Figs 10 and 12, showing the combined results of both LB and OB. As a check more fundamental comparisons were made by considering the contributions of LB and lateral-torsional buckling separately.

Figure 14 shows the relationship between LB and OB amplitudes for some representative beam lengths

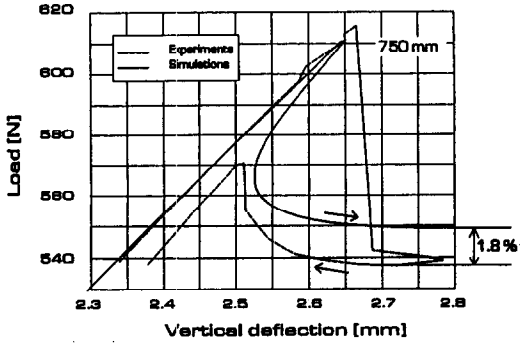

Fig. 13. Detail of Fig. 10 for the 750 mm beam.

and it provides more insight into post-buckling behavior than Fig. 12. It must be noted that the difference between this figure and Figs 1 and 2 relates to amplitude. Figures 1 and 2 include the dimensionless amplitudes of normalized buckling modes, while in Fig. 14 amplitude means the maximum deflection of the edge of the real flange. The curves illustrate the coupling between LB and OB. When the LB load is the smaller, the equilibrium path has a vertical tangent at the origin, indicating only LB of the flange, which decreases the lateral stiffness. Lateral-torsional buckling did not immediately occur. Beyond the secondary bifurcation point, however, it did gradually appear. From the numerical simulation (Fig. 1), it can be seen that the second local mode was initiated at the same time. That is understandable, because as soon as lateral bending occurs, the local amplitude on the concave side should increase, whereas the local amplitude on the convex side should diminish.

The longer profiles started with overall lateral-torsional buckling, which compressed the flange half on the concave side of the beam. At the secondary bifurcation point, LB begins and, from Fig. 2, it can be seen that both local modes are involved immediately.

Figure 14 shows a closer agreement between the experimental and numerical results for the shorter beams, probably due to a shorter beam starting with a stable local plate buckling, which implies that a small load increase was accompanied by a relatively small LB amplitude increase. A longer beam, however, started with almost neutral buckling, implying that a small change in the load caused a relatively large increase in OB amplitude. As a consequence, small differences in the calculated buckling load, together with small imperfections in the test specimen, would cause larger differences between the calculated and measured amplitudes.

6. CONCLUSIONS

A spline finite element program for the initial post-buckling analysis of linear elastic prismatic plate

structures was developed. Critical loads and modes are obtained in much the same way as with other programs; however, the post-buckling approach results in a set of non-linear equations expressed by the amplitudes of the relevant buckling modes. The numerical simulations and laboratory experiments confirmed that it is possible to describe initial post-buckling behavior that comprises non-linear mode interactions with a few buckling modes. However, selecting the appropriate modes from all the modes obtained numerically requires an insight into the relevant buckling phenomenon. The reduced potential energy expression obtained with the numerical model, together with the evolution of a limited number of amplitudes as functions of the load, provided a better insight than a continuation method applied to a full set of finite element equations. Moreover, a small set of non-linear equations expressed in the amplitudes can be solved faster than a large set expressed in all the nodal displacements.

The ideas presented here have been implemented in the FEMME program at Helsinki University of Technology by R. J. Kouhia and in the DIANA program of TNO Building and Construction Research (Delft) by G. M. A. Schreppers.

Acknowledgements—This project was supported by the Dutch Technology Foundation (STW). Calculations were done on a Challenge computer (Silicon Graphics) in the Faculty of Mechanical Engineering. The test specimen were produced by the Dutch Aerospace Laboratory (NLR, Emmeloord).

REFERENCES

1. J. M. T. Thompson and G. W. Hunt, *A General Theory of Elastic Stability*. Wiley, Chichester (1984).
2. W. T. Koiter, Over de Stabiliteit van het Elastisch Evenwicht (in Dutch). Ph.D. Thesis, Delft University of Technology (1945). [English translations: NASA TT F10, 833 (1967) and AFFDL, TR-7025 (1970).]
3. G. Augusti, Stabilita di Struttura Elastiche Elementari in Presenza di Grandi Sportamenti. *Acad. Sci. Fis. Mat.* **4**(5), Napoli, Serie 34 (1964).
4. D. Bushnell, Buckling of shells—pitfalls for designers. *AIAA J.* **19**, 1183–1226 (1981).
5. G. M. van Erp and C. M. Menken, Initial post-buckling analysis with the spline finite strip method. *Comput. Struct.* **40**, 1185–1191 (1991).
6. E. Byskov and J. W. Hutchinson, Mode interaction in axially stiffened cylindrical shells. *AIAA J.* **15**, 941–948 (1977).
7. W. T. Koiter, Current trends in the theory of buckling. In: *IUTAM Symp. Buckling of Structures*, Harvard University, pp. 1–16. Springer, Berlin (1974).
8. C. M. Menken, W. J. Groot and G. A. J. Stallenberg, Interactive buckling of beams in bending. *Thin-Walled Struct.* **12**, 415–434 (1991).
9. G. M. van Erp, Advanced buckling analysis of beams with arbitrary cross sections. Ph.D. Thesis, Eindhoven University of Technology (1989).
10. R. Kouhia and C. M. Menken, On the solution of second order post-buckling fields. *Numer. Meth. Engng* **11**, 443–453 (1995).
11. R. Kouhia and C. M. Menken, On the discretization strategy in the analysis of plated thin-walled structures. In: *Numerical Methods in Engineering '92* (Edited by Ch. Hirsch *et al.*), pp. 413–419. Elsevier Science, Amsterdam (1992).
12. R. Kouhia, C. M. Menken, M. Mikkola and G. M. A. Schreppers, Computing and understanding interactive buckling. In: *Proc. 5th Finnish Mechanics Days* (Edited by R. A. E. Makinen and P. Neittaanmaki, pp. 53–60. University of Jyvaskyla, Department of Mathematics, Laboratory of Scientific Computing, Report 3/1944 (1994).
13. J. H. Starnes, N. F. Knight and M. Rouse, Post-buckling behavior of selected flat graphite–epoxy panels loaded in compression. *AIAA J.* **13**, 1236–1246 (1985).
14. J. M. Davies and P. O. Thomasson, Local and overall buckling of light gage members. In: *Instability and Plastic Collapse of Steel Structures* (Edited by L. J. Morris), pp. 479–492. Granada, London (1983).
15. R. Benito, Static and dynamic buckling of plate assemblies. Thesis submitted in partial fulfillment of the requirements of DSc degree of the Washington University of St Louis (1983).
16. S. Sridharan and R. Benito, Static and dynamic interactive buckling. *J. Engng Mech. ASCE*, **110**, 49–65 (1984).
17. C. M. Menken, W. J. Groot and R. Petterson, Experiments on coupled structural instabilities. Paper presented at the *10th Int. Conf. Experimental Mechanics*, Lisbon, 18–22 July (1994).
18. A. J. Reis, Some comments on mode interaction in thin walled beams. In: *Sec. Int. Coll. on Stability of Steel Structures*, Final Report, Liege, Belgium, pp. 243–245.